Low-energy positron scattering from gas-phase pyrimidine: A quantum treatment of the dynamics and a comparison with experiments

J. Franz*
Mulliken Center for Theoretical Chemistry, University of Bonn, Beringstr. 4-6, D-53115 Bonn, Germany

F. A. Gianturco
Department of Chemistry, The University of Rome Sapienza, Piazzale A. Moro 5, I-00185 Rome, Italy
(Received 25 June 2013; published 24 October 2013)

In the present work we are reporting detailed quantum scattering calculations that describe the diffusion of a beam of low-energy positrons interacting with the pyrimidine target as a gas-phase partner. The calculations have employed an essentially *ab initio* model for the short-range correlation interaction and for the electrostatic interaction of an impinging positron and the electron+nuclear structure of the target molecule at its equilibrium geometry. The available experiments were also performed in the low-energy region below about 30 eV and have been reported by two different experimental groups cited in the main text. Those data include integral elastic plus rotationally and vibrationally summed cross sections, together with angular distributions over the same range of energies. The effects on the scattering observables which stem from the permanent dipole moment of the title molecule are carefully analyzed and computational corrections which ensure numerical convergence are introduced and discussed. The additional uncertainties introduced by the angular discrimination error present in the experiments are also discussed and analyzed, thereby providing a numerical procedure for correcting all available data. The final comparison between experimental angular distributions and the computed counterparts produced in the present work turns out to be very good. The same applies to the comparison in size and energy dependence of the integral cross sections, where we show that our calculated quantities and the corrected experiments are in very good agreement over the whole range of available energies.

DOI: 10.1103/PhysRevA.88.042711 PACS number(s): 34.80.Bm, 87.14.gn, 87.57.uk

I. INTRODUCTION

The interactions of positrons, the electron's antiparticle, with biological material plays an important role in nuclear medicine [1]. The positrons can be created by positron-electron pair production or by nuclear β^+ decay [1]. Electron-positron pair production can be triggered by the interaction of high-energy photons with the electromagnetic field of an atomic nucleus. The photon energy has to be at least the threshold energy of 2×511 keV $= 1.022$ MeV, which is the energy equivalent to the rest mass of the two particles. The process of creating positrons by nuclear β^+ decay is used in positron emission tomography (PET), where specific molecules are marked with β^+ emitters. For applications in nuclear medicine it is important to know about the interactions of the positron with biological material, from its creation until its annihilation, either the direct interactions with a molecular bound electron, or the secondary interactions which can occur after forming positronium. In this context, therefore, the knowledge of the interaction of slow positrons, with kinetic energies below 30 eV with biomolecules is certainly an important item for developing any model for the involved processes. It thus follows that a fairly large number of experiments have been analyzing beams of slow positrons colliding with individual biomolecules in the gas phase. It is important to note here that in these collision experiments the linear transmission technique is used, and therefore it is not possible to distinguish between unscattered positrons and positrons scattered elastically into a small cone of forward direction. Due to this effect, the amount of unscattered particles is usually overestimated in the measurements and consequently the total elastic cross sections become affected by very large uncertainties. The availability of reliable computations thus becomes an essential step on the way to get a better knowledge of the overall collision process. One biomolecule of very broad interest in many areas of biomaterial studies is indeed the pyrimidine. It has structural similarities with the nuclear bases uracil, thymine, and cytosine and is important in the biochemistry of the reactions involving such nuclear bases [2].

In this paper we shall therefore report new quantum computations of the rotational elastic and inelastic cross sections of low-energy positrons colliding with pyrimidine. On the experimental side, the cross sections for slow positrons in collision with pyrimidine have been measured recently by Zecca *et al.* [3] and by Palihawadana *et al.* [4]: In these experiments the measured elastic integral cross sections disagree with each other. Palihawadana *et al.* [4] are also presenting differential cross sections so we shall also compute such quantities for further comparisons.

In our computations we do not take into account inelastic channels like positronium formation, annihilation, ionization, and vibrational or electronic excitation, because such a treatment is computationally too demanding. Annihilation is possible at all collision energies. The coupling between elastic channels and annihilation is usually small and annihilation is usually treated uncoupled from elastic scattering (see, e.g., Chapter 4.2 in [5] and Humberston *et al.* [6]) The couplings between open channels usually will give structure in the elastic cross section on either side of each threshold for opening a

*Present address: Department of Atomic, Molecular and Optical Physics, Faculty of Applied Physics and Mathematics, Gdansk University of Technology, ul. Narutowicza 11/12, PL 80-233 Gdansk, Poland; j.franz@ucl.ac.uk

new inelastic channel. A detailed discussion can be found in Charlton and Humberston [5]. The effects on the structure of the elastic cross section can be expected to be much smaller than the experimental uncertainties. Therefore it should be a valid assumption to neglect these channels in the comparison of elastic cross sections. The threshold for positronium formation is given by $E_{\rm Ps} = E_{\rm ion} - 6.8$ eV [5]. The experimental value for the first ionization energy (at the peak maximum) was measured by Potts *et al*. [7] to be $E_{\rm ion} \approx 9.8$ eV, which gives $E_{\rm Ps} \approx 3.0$ eV.

This paper is organized in the following way: In the next section we describe our theoretical model and our computational procedure. In Sec. III we compare our computations with the experimental differential and integral cross sections and, to improve on this comparison, we further add the computed partial cross section for the forward scattering which are corrected for the effects originating from the angular discrimination correction. The paper ends with presenting our conclusions in Sec. IV.

II. THEORETICAL AND COMPUTATIONAL METHODS

A. Scattering equations

In order to obtain the scattering cross sections for polyatomic molecules, we need to solve the Schrödinger equation of the total system,

$$(H - E)\Psi = 0, \tag{1}$$

at the total energy E, for the corresponding wave function Ψ. Here H is the total Hamiltonian given by

$$H = H_{\rm mol} + K + V, \tag{2}$$

where $H_{\rm mol}, K$, and V represent the operators of the molecular Hamiltonian, kinetic energy for the scattered positron, and the interaction potential between the incident positron and the target molecule, respectively. The $H_{\rm mol}$ further consists, in general, of the rotational and vibrational parts,

$$H_{\rm mol} = H_{\rm rot} + H_{\rm vib}, \tag{3}$$

whereby we exclude, at the collision energies considered, electronic excitations, ionization, and the Ps formation channels.

The total wave function Ψ is described in the body-fixed (BF) reference frame, in which the z axis is taken along the direction of the main molecular axis and is expanded around a single-center (SCE) as

$$\Psi(\mathbf{r}_1 ... \mathbf{r}_Z, \mathbf{r}_p|\mathbf{R}) = \Psi_{\rm mol}(\mathbf{r}_1 ... \mathbf{r}_Z|\mathbf{R})\varphi(\mathbf{r}_p|\mathbf{R}), \tag{4}$$

where

$$\varphi(\mathbf{r_p}|\mathbf{R}) = \sum_{l\pi\mu h} r_p^{-1} u_{lh}^{\pi\mu}(r_p|\mathbf{R}) X_{hl}^{\pi\mu}(\hat{\mathbf{r}}_p). \tag{5}$$

In Eq. (4), $\mathbf{r_i}$ represents the position vector of the ith electron among the Z bound electrons in the target, taken from the center of mass. $\Psi_{\rm mol}$ is the electronic wave function for the molecular target at the nuclear geometry $\mathbf{R}$. The continuum function $\varphi(\mathbf{r_p}|\mathbf{R})$ refers to the wave function of the scattered positron under the full action of the field created by the molecular electrons and by their response to the impinging positron as described in [8]. Each $u_{lh}^{\pi\mu}$ is the radial part of the wave function for the incident particle and the $X_{hl}^{\pi\mu}$ are the symmetry-adapted angular basis functions (for more detailed information see, e.g., [9]). The suffix π stands for the irreducible representation (IR), μ distinguishes the components of the basis, if its dimension is greater than one, and h does the same within the same set with angular momentum quantum number l.

We can now assume that the target molecule can be kept fixed during the collision, since the molecular rotations and vibrations are often slower when compared with the velocity of the impinging positrons considered in the present study. This is called the fixed-nuclear (FN) approximation [10] that ignores the molecular term of $H_{\rm mol}$ in Eq. (2) and fixes the values of all $\mathbf{R}$ at their equilibrium locations in the target molecule. To solve the Schrödinger equation in the FN approximation, we make use of the body-fixed (BF) system rather than the laboratory frame, space-fixed (SF) frame of reference, because a formulation in the former can be simpler, both conceptually and computationally. The two systems are related through a frame transformation scheme given, for example, by Chang and Fano [10].

After substituting Eq. (4) into Eq. (1) under the FN approximation, we obtain a set of coupled differential equations for u_{lv} where, for simplicity, v represents $(\pi\mu h)$ collectively:

$$\left\{\frac{d^2}{dr_p^2} - \frac{l(l+1)}{r_p^2} + k^2\right\} u_{lv}(r_p|\mathbf{R}) = 2\sum_{l'v'} \langle lv|\mathbf{V}|l'v'\rangle u_{l'v'}(r_p|\mathbf{R}), \tag{6}$$

with

$$\langle lv|\mathbf{V}|l'v'\rangle = \int d\hat{r}_p X_{lv}^*(\hat{r}_p) V(r_p|\mathbf{R}) X_{l'v'}(\hat{r}_p). \tag{7}$$

When solving Eq. (6) under the boundary conditions that the asymptotic form of u_{lv} is represented by a sum containing outgoing spherical Bessel and Neumann functions we obtain the corresponding S-matrix elements $S_{l'v'}^{lv}$. The actual numerical procedure we have employed to solve that equation is given in detail in [11,12].

The integral cross section (ICS) for the elastic scattering in the BF frame is given by

$$\sigma_{cc} = \frac{\pi}{k^2} \sum_{lv} \sum_{l'v'} \left|T_{l'v'}^{lv}\right|^2, \tag{8}$$

where the index cc indicates the close-coupling approach.

The $\mathbf{T}$-matrix is defined as a function of the $\mathbf{S}$ and $\mathbf{K}$ matrices,

$$\mathbf{T} = 1 - \mathbf{S} \tag{9}$$

$$= 1 - (1 - i\mathbf{K}) \cdot (1 + i\mathbf{K})^{-1}. \tag{10}$$

The integral cross section diverges in the forward direction in the presence of a molecular dipole moment, because of the long-range interaction between the positron and the molecular dipole moment. This problem can be solved by applying the following closure formula for the differential cross section [21]:

$$\frac{d\sigma}{d\Omega}(J\tau \to J'\tau') = \frac{d\sigma_{\rm rd}^B}{d\Omega}(J\tau \to J'\tau') + \sum_L \left(A_L - A_L^B\right) P_L(\cos\theta), \tag{11}$$

where $J\tau$ and $J'\tau'$ denote the initial and final rotational level, respectively. The first quantity on the right-hand side is the differential cross section for a rotating dipole using the first Born approximation. The $P_L(\cos\theta)$ are the Legendre functions. The coefficients A_L are computed from the **K** matrices, which are obtained by solving the close-coupling equations. The coefficients A_L^B are computed from the **K** matrices using the first Born approximation. Explicit formulas for A_L and A_L^B are given in Gianturco and Jain [9]. The final differential cross section is obtained by summation over the different initial and final rotational levels,

$$\frac{d\sigma}{d\Omega} = \sum_{J\tau J'\tau'} w_J \frac{d\sigma}{d\Omega}(J\tau \to J'\tau'), \tag{12}$$

where w_J is the relative occupation of the initial rotational level J. The corresponding integral cross section in the SF frame can be computed as

$$\sigma = \sigma_{rd}^B + \sigma_{cc} - \sigma_{fd}^B. \tag{13}$$

Here σ_{rd}^B is the integral cross section for a rotating dipole in the Born approximation. σ_{cc} is the integral cross section obtained by solving the close-coupling equations in the FN approximation and σ_{fd}^B is the integral cross section for a fixed dipole. Further details can be found in Sanna and Gianturco [21].

B. The DFT modeling of correlation and polarization

The interaction between the positron and the molecular nuclei and electrons is specified by the total interaction potential:

$$V_{\rm tot}(\mathbf{r}_e|\mathbf{R}) = V_{\rm st}(\mathbf{r}_e|\mathbf{R}) + V_{\rm pcp}(\mathbf{r}_e|\mathbf{R}), \tag{14}$$

which is the sum of the static potential $V_{\rm st}$ and the correlation-polarization potential $V_{\rm pcp}$. The static potential $V_{\rm st}$ is the exact electrostatic interaction potential between the positron and the nuclei and electrons in the molecule. The correlation-polarization potential is modeled by the potential [12]:

$$V_{\rm pcp}(\mathbf{r}_e|\mathbf{R}) = \begin{cases} V_{\rm corr}(\mathbf{r}_e|\mathbf{R}) & \text{for} \quad r_p \leqslant r_c \\ V_{\rm pol}(\mathbf{r}_e|\mathbf{R}) & \text{for} \quad r_p > r_c \end{cases}. \tag{15}$$

Here $V_{\rm corr}$ and $V_{\rm pol}$ are the short-range part and long-range parts of the correlation-polarization potential. r_c is the outermost point, at which $V_{\rm pol}$ becomes larger than $V_{\rm corr}$. $V_{\rm corr}$ is based on the functional $\epsilon^{\rm e-p}[\rho(\mathbf{r}_e|\mathbf{R})]$ for the correlation energy of one positron in an electron gas with density $\rho(\mathbf{r}_e|\mathbf{R})$. Boronski and Nieminen [13] have derived interpolation formulas for $\epsilon^{\rm e-p}$. $V_{\rm corr}$ can be obtained from $\epsilon^{\rm e-p}$ by the functional derivative [12]:

$$V_{\rm corr}(\mathbf{r}_e|\mathbf{R}) = \frac{\delta}{\delta\rho}\{\epsilon^{\rm e-p}[\rho(\mathbf{r}_e|\mathbf{R})]\}. \tag{16}$$

The long-range part $V_{\rm pol}$ of the correlation-polarization potential is given by

$$V_{\rm pol}(\mathbf{r}_e|\mathbf{R}) = -\left(\frac{\alpha_0}{2r^4} + \frac{\alpha_2}{2r^4}P_2(\cos\theta)\right), \tag{17}$$

where α_0 and α_2 are the values of the isotropic and anisotropic polarizabilities, respectively, and $P_2(\cos\theta)$ is a Legendre polynomial.

C. Computational details

The target molecule is constrained to its equilibrium structure that belongs to the C_{2v} symmetry. The molecular geometry and the ground-state molecular orbitals are generated with the GAUSSIAN 09 program package employing the PBE density functional and aug-cc-pVTZ basis set [14]. The computed molecular dipole moment is 2.32 Debye, which compares well with the experimental value of 2.28 Debye listed in Vaughan [15]. Our computed rotational constants are $A = 6.25$ GHz, $B = 6.04$ GHz, and $C = 3.08$ GHz. This is in good agreement with the corresponding experimental values of Kisiel *et al.* [16]: 6.28, 6.07, and 3.08 GHz. With the PBE functional the elements of the polarizability tensor are computed to be $\alpha_{xx} = 37.7$ bohr^3, $\alpha_{yy} = 69.8$ bohr^3, and $\alpha_{zz} = 73.1$ bohr^3. These values are in good agreement with computations by Hättig *et al.* [17] (31.5, 67.8, and 70.2 bohr^3) using *ab initio* coupled cluster response theory and computations by Jansik *et al.* [18] (37.0, 67.9, and 70.6 bohr^3) using the B3LYP functional. The isotropic polarizability can be obtained by $\alpha_0 = \frac{1}{3}(\alpha_{xx} + \alpha_{yy} + \alpha_{zz})$, and the anisotropic polarizability by $\alpha_2 = -\alpha_{xx} + \frac{1}{2}(\alpha_{yy} + \alpha_{zz})$.

The single-center expansions of the molecular electron density and of the potential are done with an improved version of the SCELIB3.0 computational library [19], to which we have added the correlation-polarization potential specific for modeling the interactions of the molecular electrons with slow positrons. The coupled scattering equations are solved by Volterra integration, using an improved version of the VOLSCAT program package [20]. More specifically the VOLSCAT suite of codes computes the integral cross section in the BF frame (denoted previously as σ_{cc}) and therefore generates the necessary body-fixed **K** matrices.

The body-fixed **K** matrices are then processed by the program package POLYDCS [21], another in-house suite of codes, that transforms the body-fixed **K** matrices into the space-fixed **K** matrices and further applies the Born correction, as outlined in our earlier publication by Sanna and Gianturco [21]. From the space-fixed **K** matrices obtained in this way we can further generate the state-to-state rotationally elastic and inelastic differential and integral cross sections. During the frame transformation step of the present calculations the rotational eigenfunctions and eigenvalues for the asymmetric top are in turn generated using the program ASYMTOP of Jain and Thompson [22] with our computed rotational constants.

III. RESULTS AND DISCUSSION

A. Differential cross sections

In Figs. 1–6 the experimental and computed differential cross sections (DCS) are reported for collision energies of 1, 3, 6, 10, 14, and 20 eV. In Fig. 5 the computed DCS at 14.0 eV is compared with the experimental DCS at 15.0 eV. At all other energies the computations are done for the same energies as in the experiments. The scattering machine at ANU produces differential cross sections, that are folded at 90° (i.e., the value shown at 80° is the sum of the values at 80° and 100°). Therefore we folded our computed data also at 90° and the same with the theoretical data given in Palihawadana *et al.* [4]. The data of Palihawadana *et al.* [4] are shown by

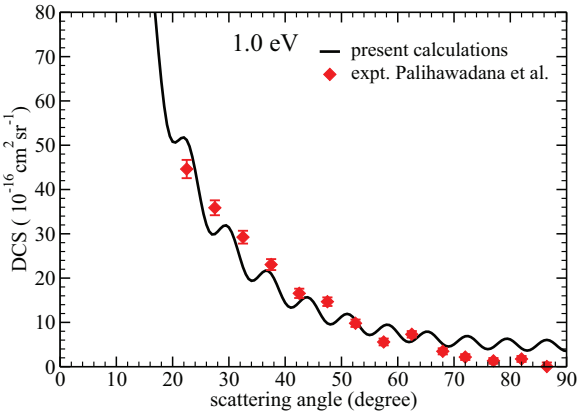

FIG. 1. (Color online) Differential cross sections (DCS) for positron scattering off gas-phase pyrimidine at a collision energy of 1.0 eV. The DCS is folded at 90°. Computed results are shown by the solid black line. The experimental data by Palihawadana *et al*. [4] is given by the red diamonds. See text for more details.

the red diamonds. The error bars show the statistical errors of the experiments, but not their total error. The uncertainty in the energy is estimated to be ± 25 meV [4]. Our computed differential cross section is given by the solid black line.

In all cross sections one can easily see the strong increase of these cross sections in the forward scattering direction, i.e., at smaller angles. It is reassuring to see that the shape and magnitude of the two compared cross sections are in good agreement with each other.

At all energies the experiments have slightly higher values than the theory for scattering angles below about 30°.

The experiments were performed by temperatures of 24° ± 2°C. Due to the finite energy resolution in the experiments, rotational and vibrational inelastic collisions cannot be distinguished from elastic collisions. In our computations we are considering only rotational transitions from the rotational ground state into the lowest five rotational levels. Therefore the rotational temperature in our computations is 0 K. Furthermore we do not consider any vibrational inelastic processes. However, we estimate these effects to be small in comparison with the experimental uncertainties. In the appendix we show that for a rigid rotor with the same parameters as the molecule

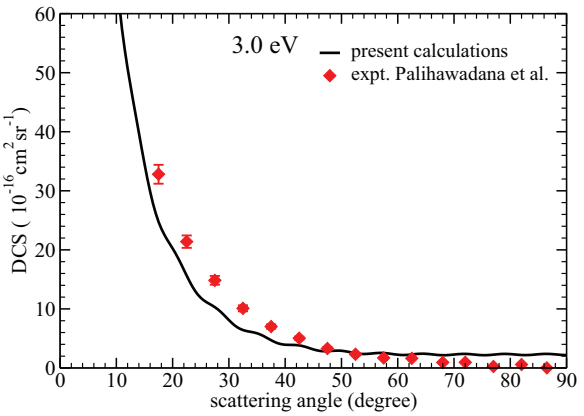

FIG. 2. (Color online) Same as Fig. 1 for a collision energy of 3.0 eV.

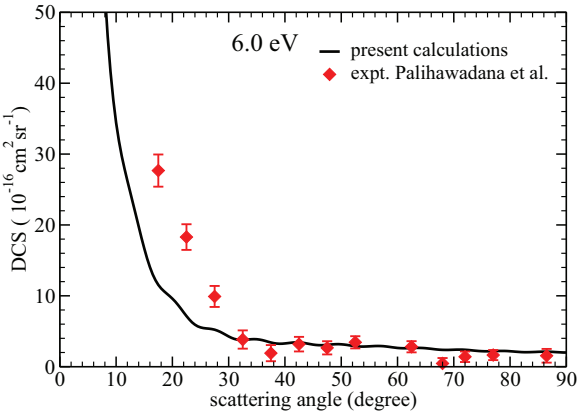

FIG. 3. (Color online) Same as Fig. 1 for a collision energy of 6.0 eV.

under consideration, the temperature effects are rather small for collisional energies between 1 and 20 eV.

On the whole, however, we can say that the present calculations follow rather closely, both in size and angular behavior, the existing experimental DCS for the present system.

B. Integral cross sections

Figure 7 now reports the computed integral cross sections for various partial wave expansions that we have tested in the present computational runs. The thick lines in the lower part of the panel show the cross sections computed in the BF frame, while the thin lines show the integral cross sections after applying the Born dipole correction in the SF reference frame and summing over the rotational elastic and inelastic channels as described in detail in the POLYDCS code [21]. When performing the summation over rotational channels, the zeroth level is included as the initial state and the first five states are also included as final rotational channels. One can see that the convergence of the results in the body frame is fairly slow with respect to the partial wave expansion: This slow convergence with respect to the increase in size of the partial wave expansion is well known for molecular systems with large permanent dipole moments. In the SF calculation we also clearly see that

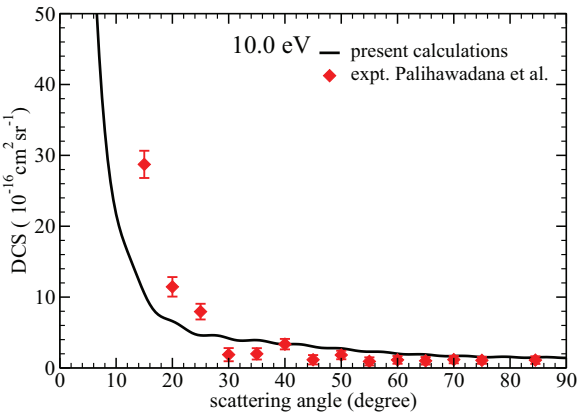

FIG. 4. (Color online) Same as Fig. 1 for a collision energy of 10.0 eV.

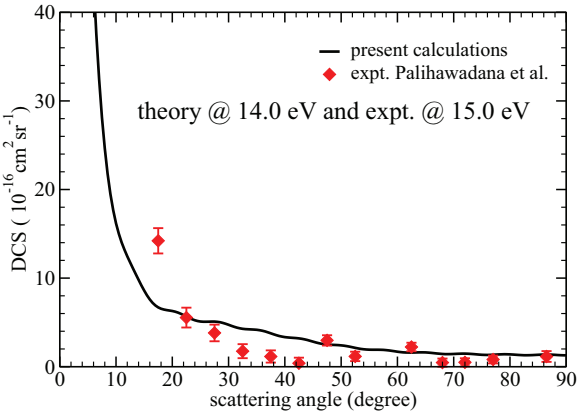

FIG. 5. (Color online) Same as Fig. 1, but showing calculations at collision energy of 14.0 eV and experimental data at 15.0 eV.

all the computed cross sections are instead very close to each other and the convergence with respect to the partial wave expansion is occurring much faster. In fact, the results for $l_{max} = 20$ are nearly coincident with the results for $l_{max} = 50$.

In Fig. 8 our computational results are compared with the experimental ICS of Zecca *et al*. [3] and two sets of data measured Palihawadana *et al*. [4]. The experimental raw data is shown by the solid symbols with error bars. The open symbols show the experimental data after doing the correction for forward scattering, which is described below.

In our computations, shown by the solid black line, we use the partial wave expansion up to $l_{max} = 50$ and include the Born dipole correction. The results are therefore obtained within the SF frame as discussed before and we therefore carried out a summation over all the rotational elastic and inelastic channels included to reach convergence in the expansion.

All the experimental cross section, discussed below as elastic integral cross sections also contain contributions, not resolved, from transitions to the accessible rotational and vibrational inelastic channels: This is due to the limited energy resolution of the experimental setups used by Zecca *et al*. [3] and Palihawadana *et al*. [4].

The experimental data by Zecca *et al*. [3] are shown by the red circles. The paper by Palihawadana *et al*. [4] actually contains two sets of data, which can be used to represent the

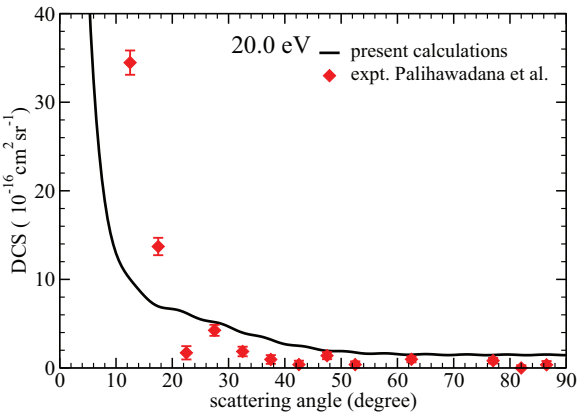

FIG. 6. (Color online) Same as Fig. 1 for a collision energy of 20.0 eV.

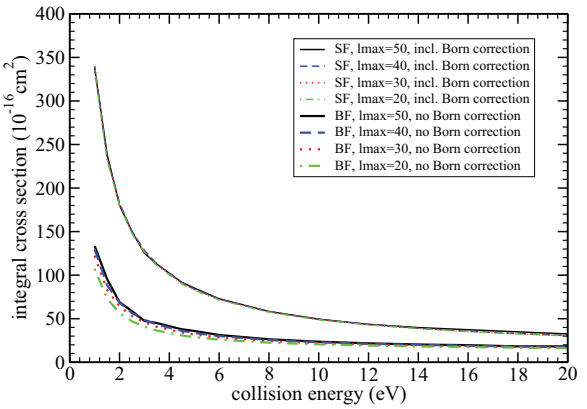

FIG. 7. (Color online) Computed integral cross sections for positron scattering off gas-phase pyrimidine using different partial wave expansions. The thick lines in the lower part represent computations in the body-fixed (BF) frame. The thin lines are the calculations done in the space-fixed (SF) frame including Born dipole correction and summation over rotational elastic and inelastic channels.

elastic integral cross sections. The data shown by the blue diamonds have been calculated as

$$\sigma_E^{diff} = \sigma_T - \sigma_{Ps} - \sigma_I, \tag{18}$$

which we obtained by subtracting the measured cross sections for positronium formation σ_{Ps} and ionization σ_I from the measured total cross sections σ_T. The error bars shown are the statistical errors ($\Delta\sigma_T$) given in Palihawadana *et al*. [4] for the total cross sections. The paper by Palihawadana *et al*. [4] contains another set of data from a direct measurement of the elastic integral cross sections, which is shown by the solid green squares.

All the experiments are using a linear transmission technique. Scattering events with a scattering angle smaller than a certain angle θ_{min} cannot be distinguished from the unscattered particles of the positron beam. Therefore in the linear transmission experiments all scattering events within this angular cone in forward direction are missing in the elastic

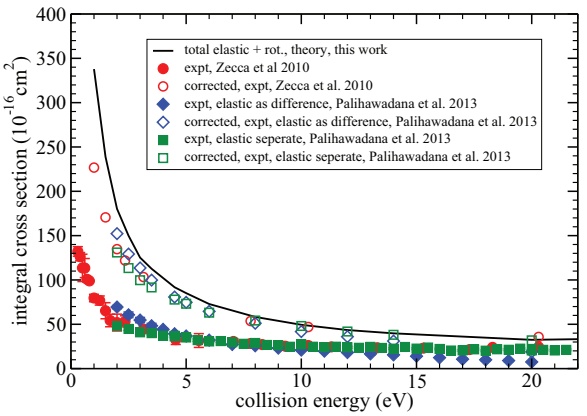

FIG. 8. (Color online) Computed and measured elastic integral cross sections for positron scattering. The new computational data are shown by the solid black line. The uncorrected experimental data are shown by solid symbols, the corrected experimental data by open symbols. (Zecca *et al*. [3], red circles; Palihawadana *et al*. [4], blue diamonds and green squares). See text for further details.

cross sections (see, e.g., Sullivan *et al*. [23] for a general discussion). The scattering machines in Trento and at ANU are using a retarding potential technique. For such a machine Kauppila *et al*. [24] and Kwan *et al*. [25] are suggesting to estimate the angle $\theta_{\min}$ as a function of the retarding potential ΔV and the collision energy E by the following relation:

$$\theta_{\min} = \sin^{-1}\sqrt{\frac{e\Delta V}{E}}. \tag{19}$$

Here e is the elementary charge. The physical idea behind this equation is as follows: After the collision the positron velocity has a component in axial direction and a component in transversal direction. The corresponding contributions of the kinetic energy are $E_{\text{axial}} = E\cos^2\theta$ and $E_{\text{trans}} = E\sin^2\theta$. The retarding potential is located between the scattering cell and the detector. The potential affects only the axial part of the kinetic energy. All scattered particles with a transversal kinetic energy, that is, larger than the retarding potential are reaching the detector, and, hence, are counted as unscattered particles. The minimal transversal kinetic energy for this to happen is

$$E_{\text{trans}} = e\delta V, \tag{20}$$

which gives the expression above for the angular discrimination error $\theta_{\min}$.

In order to correct the experimental data for the particles scattered into the forward cone, we have added to the experimental data the following part:

$$\sigma_{\text{E}}^{\text{forward}} = 2\pi\int_0^{\theta_{\min}} \frac{d\sigma_{\text{calc}}}{d\Omega}\sin\theta d\theta, \tag{21}$$

which contains the integral over our computed differential cross sections $\frac{d\sigma_{\text{calc}}}{d\Omega}$ carried out between the forward direction and the angular discrimination angle $\theta_{\min}$.

In the experiments by Zecca *et al*. the retarding potential is $\Delta V = 90$ mV. The experimental values of Zecca *et al*., corrected by this procedure, are given by the open red circles. Most of the experimental values we have corrected with computed data at the same energies. However, experimental data at the collision energies of 2.35, 3.15, 7.8, 10.3, 20.3, and 25.15 eV are corrected with computational data, which were carried out at the energies of 2.5, 3.0, 8.0, 10.0, 20.0, and 25.0 eV.

For the two data sets in the experiments by Palihawadana *et al*. [4] different retarding potentials have been used. In the data set, which is obtained as the difference between total cross section and the cross sections for positronium formation and ionization, the retarding potential is $\Delta V = 72.8$ mV. The corrected data points are shown by the open blue diamonds. In the direct measurement of the elastic cross section the retarding potential is $\Delta V = 378$ mV. The correction data points are shown by the open green squares.

As mentioned in the previous subsection the molecular gas in the experiments close to standard room temperature (at $24^\circ \pm 2^\circ$ C) and contains rotational and vibrational inelastic and elastic cross sections. In contrast, in our computations we do not consider vibrational effects and all molecules are initially in the rotational ground state. We estimate that at collisional energies above 1 eV these effects are rather small compared to other uncertainties in the experiments and in the modeling. A more detailed analysis of the temperature effects can be found in the Appendix.

We see that, after correcting for the angular discrimination error in the three experimental data sets, all measured data sets are in good agreement with each other and also with our present calculated values: Such a result is certainly a reassuring confirmation for the quality of the quantum scattering model we have employed. It is interesting to note that even after adding the corrections to the experimental data, the corrected data points are below the computed values, whereas in the differential cross sections the experimental values are above the computed values. One reason might be that the angular discrimination error is larger than value for $\theta_{\min}$ by using Eq. (19) and the given values for the retarding potential ΔV. Another reason might be differences in the experimental setup in the measurement of the differential and the integral cross sections and a different calibration of the absolute values.

IV. PRESENT CONCLUSIONS

This work reports quantum scattering calculations for the low-energy positron scattering from gas-phase molecules of pyrimidine. The details of our method have been provided summarily in Sec. II and indicate that one needs to pay special attention to the cross sections computed under the additional difficulties which are imposed by the presence of the permanent dipole moment in the pyrimidine target. In the recent literature we found that there are three sets of data from two different sources which report experimental determination of the integral cross sections [3,4] and one set of additional data at several energies which give experimental values for the differential cross sections [4].

The three experimental sets of integral cross sections differ in value among each other at energies below 5 eV. After correcting the experimental cross-section data for the errors related to the indeterminacy of the measured flux in the regions of the forward angle scattering, the three modified data sets are seen to be in good agreement with each other and also with our calculated cross section. The corrections for the forward angular cone turned out to be different for each data set because the angular discrimination errors in the experimental setups are in fact different in each case. We have shown that one way of introducing the necessary corrections involves an integral of the computed differential cross section over the angular cone where the actual flux is being missed in the experiments. This analysis clearly shows the importance of having computed differential cross sections available for the interactive evaluation of experimental findings. The good accord between our calculations and the three experiments, after correcting them for the above angular flux analysis, indeed further confirms the reliable quality of the experimental data by reproducing them well by using our quantum method.

We further show the remarkable reliability of our computed differential cross sections in Sec. III by comparing them in some detail with the available experimental DCS of Palihawadana *et al*. [4]. We found, in fact, that the overall agreement between measured and computed DCS data is rather good, even if the experimental data tend to show larger cross sections at angles between 10° and 20°, which is also the region of greater experimental difficulties in applying flux corrections to the measured intensity of the beam of positrons.

ACKNOWLEDGMENTS

This work was carried out under the HPC-EUROPA2 project (Project No. 228398) with the support of the European Commission Capacities Area—Research Infrastructures Initiative. It has also been supported by the COST Action MP 1002—Nano-scale Insights into Ion Beam Cancer Therapy. The additional support of CASPUR and CINECA computational grants is gratefully acknowledged. J.F. thanks the staff at CINECA for their kind hospitality and support. We thank Isabella Baccarelli, Sergio Orlandini, Mario Tacconi, and Nico Sanna of CINECA for maintaining the SCELIB software package. We thank Luca Chiari (Flinders University and ANU Canberra) for telling us about the angular discrimination function of the machines in Trento and at ANU, which was used in the experiments by Zecca *et al*. [3] and Palihawadana *et al*. [4], respectively. Furthermore we thank Luca Chiari for making available to us the data of Palihawadana *et al*. [4] prior to publication.

APPENDIX: SIMULATION OF FINITE TEMPERATURE EFFECTS

The computed results, which are presented in the main section of the text, are valid for a temperature $T = 0$ K. In contrast the experiments have been performed with the molecular gas at room temperature.

In this Appendix we want to study the effects of a finite temperature on the total cross section. For this purpose we have set up a simple model system. The rotating molecule is represented by a rigid rotor instead of the more correct asymmetric top. The population of the rotational levels follows a Boltzmann distribution. The total cross section for a given collision energy $E_{\rm scat}$ and a given temperature T of the molecular gas is given by

$$\sigma(E_{\rm scat},T) = \frac{1}{Z}\left(\sum_{J=0}^{J_{\rm max}}(2J+1)e^{-\frac{E_J}{kT}}\sigma(E_{\rm scat},J,J+1) + \sum_{J=1}^{J_{\rm max}}(2J-1)e^{-\frac{E_J}{kT}}\sigma(E_{\rm scat},J,J-1)\right), \tag{A1}$$

where

$$Z = \sum_{J=0}^{J_{\rm max}}(2J+1)e^{-\frac{E_J}{kT}}. \tag{A2}$$

The rotational energy levels are those of the rigid rotor,

$$E_J = B_{\rm eff}J(J+1), \tag{A3}$$

where we have chosen the effective parameter $B_{\rm eff}$ so that the energy differences for the first dipole allowed rotational transition from the rotational ground state are the same for the rigid rotor and the asymmetric top as computed with the Hamiltonian of Jain and Thompson [22]. In the first Born approximation the rotational inelastic cross section caused by the dipole moment D is given by [21]

$$\sigma(E_{\rm scat},J,J') = \frac{8\pi D^2}{3k^2}\ln\frac{k+k'}{|k-k'|}, \tag{A4}$$

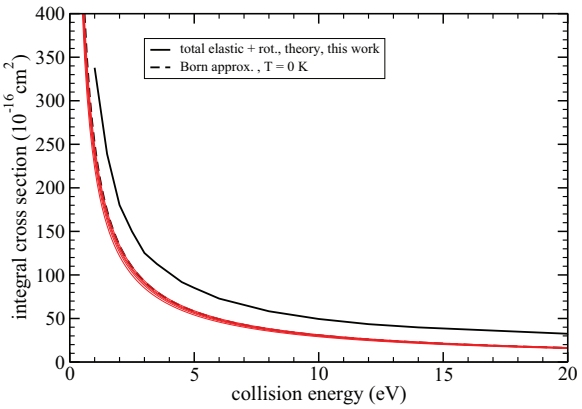

FIG. 9. (Color online) Computed integral cross sections. The close-coupling data are shown by the solid black line. The Born-dipole cross section at $T = 0$ K is shown by the broken black line. The Born-dipole cross sections for five different temperatures are shown by the thin red lines. The highest red line shows the cross section at $T = 100$ K; the following lines show the data for temperatures 200 K, 300 K, 500 K, and 1000 K.

where

$$k = \sqrt{2E_{\rm scat}}, \tag{A5}$$

and

$$k' = \sqrt{2(E_{\rm scat} + E_J - E_{J'})}. \tag{A6}$$

In Fig. 9 we compare the close-coupling results and the Born-dipole approximation at $T = 0$ K with results obtained with our simple model at five different temperatures: 100 K, 200 K, 300 K, 500 K, and 1000 K. The effects of the temperature on the Born-dipole cross section are so small, that they are hardly visible in the figure. In Fig. 10 we present the same data sets, this time using a logarithmic scale for the cross section. It can be seen that an increase of the temperature molecular gas is causing the integral cross section to decrease. In conclusion we can say that in the range of collisional energies under consideration in this study, the effect of the rotational temperature on the integral cross section should be less than one percent and therefore we neglect it in our close-coupling cross section. It should be noted that the influence of the rotational temperature will be much larger at lower collisional energies in the regime of a few meV and below.

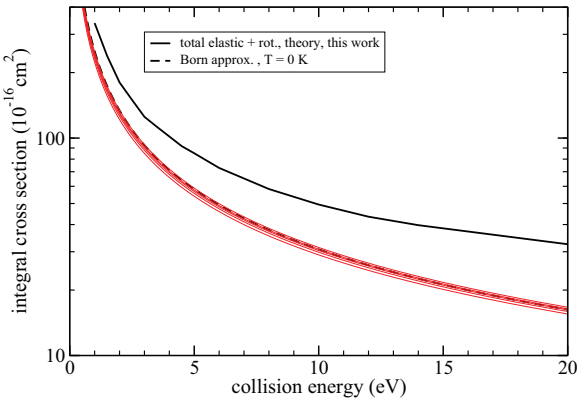

FIG. 10. (Color online) Same as Fig. 9 but in logarithmic scale.

[1] S. R. Cherry, J. A. Sorenson, and M. E. Phelps, *Physics in Nuclear Medicine*, 4th ed. (Elsevier, Philadelphia, 2012).
[2] L. Stryer, *Biochemistry*, 4th ed. (W H Freeman, New York, 1995).
[3] A. Zecca, L. Chiari, G. Garcia, F. Blanco, E. Trainotti, and M. J. Brunger, J Phys. B: At. Mol. Opt. Phys. **43**, 215204 (2010).
[4] P. Palihawadana, R. Boadle, L. Chiari, E. K. Anderson, J. R. Machacek, M. J. Brunger, S. J. Buckman, and J. P. Sullivan, Phys. Rev. A **88**, 012717 (2013).
[5] M. Charlton and J. W. Humberston, *Positron Physics* (Cambridge University Press, Cambridge, 2001).
[6] J. W. Humberston, P. Van Reeth, M. S. T. Watts, and W. E. Meyerhof, J. Phys. B: At. Mol. Opt. Phys. **30**, 2477 (1997).
[7] A. W. Potts. D. M. P. Holland, A. B. Trofimov, H. Schirmer, L. Karlsson, and K. Siegbahn, J. Phys. B: At. Mol. Opt. Phys. **36**, 3129 (2003).
[8] J. Franz, F. A. Gianturco, K. L. Baluja, J. Tennyson, R. Carey, R. Montuoro, R. R. Lucchese, T. Stoecklin, P. Nicholas, and T. L. Gibson, Nucl. Inst. Meth. B **266**, 425 (2008).
[9] F. A. Gianturco and A. Jain, Phys. Rep. **143**, 347 (1986).
[10] E. S. Chang and U. Fano, Phys. Rev. A **6**, 173 (1972).
[11] R. Curik, F. A. Gianturco, and N. Sanna, J. Phys. B: At. Mol. Opt. Phys. **33**, 2705 (2000).
[12] A. Jain and F. A. Gianturco, J. Phys. B **24**, 2387 (1991).
[13] E. Boronski and R. M. Nieminen, Phys. Rev. **34**, 3820 (1986).
[14] M. J. Frisch *et al*., computer code GAUSSIAN 09, Revision B.01, Gaussian, Inc., Wallingford, CT, 2010.
[15] W. E. Vaughan, Ed. Dig. Lit. Dielectr. **37**, 42 (1975).
[16] Z. Kisiel, L. Pszczolkwowski, J. C. Lopez, J. L. Alonso, A. Maris, and W. Caminati, J. Mol. Spectrosc. **195**, 332 (1999).
[17] C. Hättig, O. Christiansen, S. Coriani, and P. Jorgensen, J. Chem. Phys. **109**, 9237 (1998).
[18] B. Jansik, D. Jonsson, P. Salek, and H. Agren, J. Chem. Phys. **121**, 7595 (2004).
[19] N. Sanna, I. Baccarelli, and G. Morelli, Comp. Phys. Comm. **180**, 2544 (2009).
[20] N. Sanna, I. Baccarelli, and G. Morelli, Comp. Phys. Comm. **180**, 2550 (2009).
[21] N. Sanna and F. A. Gianturco, Comp. Phys. Comm. **114**, 142 (1998).
[22] A. Jain and D. G. Thompson, Comp. Phys. Comm. **32**, 367 (1984).
[23] J. P. Sullivan, C. Makochekanwa, A. Jones, P. Caradonna, D. S. Slaughter, J. Machacek, R. P. McEachran, D. W. Mueller, and S. J. Buckman, J. Phys. B: At. Mol. Opt. Phys. **44**, 035201 (2011).
[24] W. E. Kauppila, T. S. Stein, J. H. Smart, M. S. Dababneh, Y. K. Ho, J. P. Downing, and V. Pol, Phys. Rev. A **24**, 725 (1981).
[25] C. K. Kwan, W. E. Kauppila, R. A. Lukaszew, S. P. Parikh, T. S. Stein, Y. J. Wan, and M. S. Dababneh, Phys. Rev. A **44**, 1620 (1991).